The 9th of International Symposium on Transport Phenomena and
Dynamics of Rotating Machinery
Honolulu, Hawaii, February 10-14, 2002

BLOOD PUMP DEVELOPMENT USING ROCKET ENGINE FLOW SIMULATION TECHNOLOGY

Dochan Kwak
and
Cetin Kiris

NAS Applications Branch, M.S, T27B-1
NASA-Ames Research Center, Moffett Field, CA 94035

dkwak@mail.arc.nasa.gov
ckiris@mail.arc.nasa.gov

ABSTRACT

This paper reports the progress made towards developing complete blood flow simulation capability in human, especially, in the presence of artificial devices such as valves and ventricular assist devices. Devices modeling poses unique challenges different from computing the blood flow in natural hearts and arteries. There are many elements needed to quantify the flow in these devices such as flow solvers, geometry modeling including flexible walls, moving boundary procedures and physiological characterization of blood. As a first step, computational technology developed for aerospace applications was extended to the analysis and development of a ventricular assist device (VAD), i.e. a blood pump. The blood flow in a VAD is practically incompressible and Newtonian, and thus an incompressible Navier-Stokes solution procedure can be applied. A primitive variable formulation is used in conjunction with the overset grid approach to handle complex moving geometry. The primary purpose of developing the incompressible flow analysis capability was to quantify the flow in advanced turbopump for space propulsion system. The same procedure has been extended to the development of NASA-DeBakey VAD that is based on an axial blood pump. Due to massive computing requirements, high-end computing is necessary for simulating three-dimensional flow in these pumps. Computational, experimental and clinical results are presented.

INTRODUCTION

Approximately 20 million people worldwide suffer annually from congestive heart failure (CHF), a quarter of them in America alone. In the United States, an alarmingly low 2,000 to 2,500 donor hearts are available each year. One potential approach to improve this situation is to use a mechanical device to boost or to create blood flow in patients suffering from hemodynamic deterioration; that is, loss of blood pressure and lowered cardiac output. The goal of this device can be to replace the natural heart, i.e. total artificial heart, or to assist an ailing heart, i.e. ventricular assist device (VAD) [1]. In either approach, the device can be used to bridge the gap while waiting for a matching donor heart for transplantation. However, to ease the shortage of donor hearts, making these devices suitable for long-term or permanent use would be an ultimate goal.

Another benefit of an assist device is the potential for providing time for the natural heart to recover. In some patients, it has been observed that the natural heart can recover by unloading the pumping requirement through the use of a VAD. In what conditions this might happen is not very well quantified at this time and should involve physiological particulars of patients among other factors. The challenge is to design a device that can deliver the required blood circulation while not adversely impacting human physiological conditions. In this paper, since computational aspects for developing either total artificial heart or an assist device are largely the same, mechanical blood pumping devices are represented generically by a VAD.

Requirements for a VAD related to fluid dynamics are demanding such as; simplicity and reliability; small size for ease of implantation; pumping capacity to supply 5 liter/min of blood against 100 mmHg pressure; high pumping efficiency to minimize power requirements; minimum hemolysis and thrombus formation. In addition to fluid dynamic issues, there are many other important aspects to be taken care of such as material compatibility to human, controls and implantation procedures. Due to complexity of flow physics and delicate operating

conditions, empirical approach to quantify the flow phenomena in a VAD is not all that straightforward, very time consuming and expensive, especially to study many design variations. Here comes in the potential utility of computational simulation tools for the development of these devices. In this paper, the discussion is focused on how fluid dynamic issues of VAD can be resolved via computational approach.

Computational flow analysis of blood flow through mechanical devices such as VADs and artificial valves is extremely challenging [2]. Flow is unsteady and involves moving parts. For a complete analysis of a VAD such as the axial blood pump illustrated in Figure 1, human circulatory system simulation (e.g. Quarteroni [3]) has to be coupled to the device in use. However, for the purpose of developing mechanical components, a truncated circulation system can be modeled. For example, empirical inflow condition can be specified at the inlet of a VAD. Even with this type of simplifications, computational approach can produce flow field data in great detail, thus shedding lights to obtain a better understanding of the dominant flow physics produced by an artificial device. Especially, computational analysis can be utilized to optimize the design of mechanical devices at a significantly lower cost and time than required by an empirical approach. In addition to the geometric and operational complexities, these devices introduce a variety of flow phenomena, which are not normally existing in a natural heart. These include transition, turbulence, boundary layer separation, rotational effects, tip vortex and reverse flow phenomena.

In the present study, a computational procedure for developing a VAD is discussed. Since the computational tools are derived from those developed under rocket propulsion systems development, tools development on rocket turbopump will be discussed first followed by a presentation of applications to VAD flows.

FORMULATION AND METHOD OF SOLUTION

As illustrated in Figure 1, an assist device is placed to draw blood from an ailing heart and then to pump the blood into the aorta. Blood flow in large vessels as in this arrangement is believed to behave as Newtonian fluid. The flow can thus be solved by the following incompressible Navier-Stokes equations:

$$\frac{\partial u_i}{\partial x_i} = 0$$

$$\frac{\partial u_i}{\partial t} + \frac{\partial u_i u_j}{\partial x_j} = -\frac{\partial p}{\partial x_i} + \frac{\partial \tau_{ij}}{\partial x_j} + S$$

Where t is the time, x_i the Cartesian coordinates, u_i the corresponding velocity components, p the pressure, and τ_{ij} the viscous-stress tensor. When the equations are solved in a steady rotating frame of reference, the centrifugal and Coriolis forces are added as source terms to the governing equations. If the relative reference frame is moving around the x-axis, the source term, S, is given by

$$S = \begin{bmatrix} 0 \\ 0 \\ \Omega(\Omega y + 2w) \\ \Omega(\Omega z - 2v) \end{bmatrix}$$

Where Ω is the rotational speed. Relative velocity components are written in terms of absolute velocity components u_a, v_a, w_a.

$$u = u_a$$

$$v = v_a + \Omega z$$

$$w = w_a - \Omega y$$

For component analysis, rotational steady formulation may provide quick yet valuable approximate solutions. Solution procedures and a family of flow solver codes, INS3D, has been developed at NASA Ames Research Center [4-6]. This code has been applied to numerous viscous internal flow problems including turbopump component analysis for liquid rocket engine.

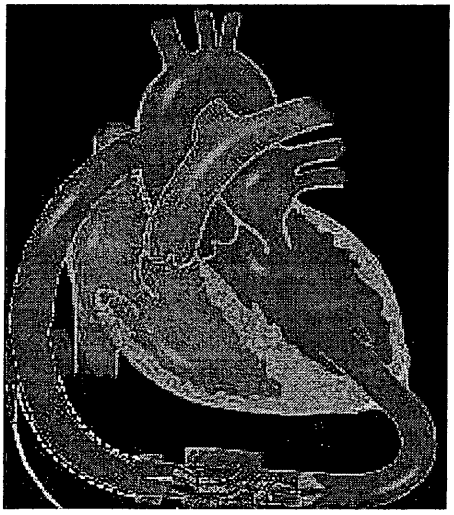

Figure 1. Schematic of a VAD based on an axial-flow pump.

The algorithm used in the current work is based on the method of pseudo-compressibility where the time-derivative of pressure is introduced into the continuity equation. The elliptic-parabolic type partial differential equations are transformed into the hyperbolic-parabolic type. Since the convective terms of the resulting equations are hyperbolic, upwind differencing can be applied to these terms. Third- and fifth-order flux-difference splitting is used for the convective terms. The upwind differencing leads to a more diagonally dominant system than does central differencing and does not require any user specified artificial dissipation. The viscous flux derivatives are computed using central differencing. In the steady-state formulation, the

time derivatives are differenced using the Euler backward formula. The equations are solved iteratively in pseudo-time until the solution converges to a steady state. In the time-accurate formulation, the equations are iterated to convergence in pseudo-time for each physical time step until the divergence of the velocity field is reduced below a specified tolerance value. Discretization of the governing equations results in a matrix equation that is solved iteratively using a non-factored Gauss-Seidel type line relaxation scheme that allows the use of a large pseudo-time step. Details of the numerical method can be found in the references cited.

CFD TECHNOLOGY FOR LIQUID ROCKET PUMP

Until recently, the high performance pump design process was not significantly different from that of 30 years ago. During the past 30 years a vast amount of experimental and operational experience has demonstrated that there are many important features of pump flows, which are not accounted for in the semi-empirical design process. Pumps being designed today are no more technologically advanced than those designed for the Space Shuttle Main Engine (SSME). During that same time span huge strides have been made in computers, in numerical algorithms, and in physical modeling.

Rocket pumps involve full and partial blades, tip leakage and exit boundary to diffuser. In addition to the geometric complexities, a variety of flow phenomena are encountered in turbopump flows. These include turbulent boundary layer separation, wakes, transition, tip vortex resolution, three-dimensional effects, and Reynolds numbers effects. In order to increase the role of Computational Fluid Dynamics (CFD) in the design process, the CFD analysis tools must be evaluated and validated so that designers gain confidence in their use.

As a part of extending the CFD technology to pump design work, INS3D code has been validated for pump component analysis using data from a rocket pump inducer [7]. The resulting computational procedure was applied to the flow through the SSME High Pressure Fuel Turbopump impeller and to the development of an advanced pump impeller (Kiris and Kwak, 1994 [8]). The results from the advanced pump impeller flow analysis are presented next.

In Figure 2, a cross sectional view of an advanced impeller is shown schematically. The computational model of an advanced pump includes the impeller and the exit shroud cavity region. Figure 3 shows the computational grid near the hub region of the impeller. The impeller design flow rate is 1,205 gal/min with a design speed of 6,322 rpm. The Reynolds Number for this calculation was 181,283 per inch. In Figure 4, the meridional velocity is shown at the impeller discharge.

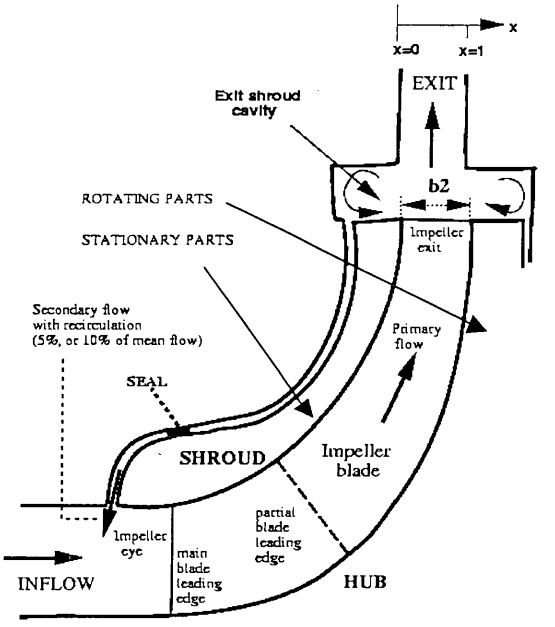

Figure 2. Schematic of an advanced pump impeller cross-section.

A relative x-distance is measured from the shroud to hub, where x=1.0 is the hub. The meridional velocities, *Cm*, were integrated along a radial strip for each constant x- position and they were non-dimensionalized by the wheel speed of 249.5 ft/sec.

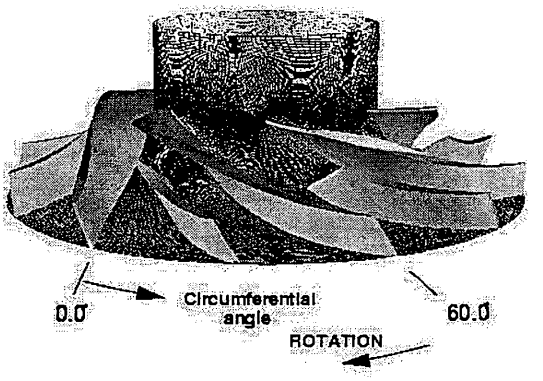

Figure 3. Advanced pump impeller computational grid on the hub surface.

The meridional velocity distribution for 5% and 10% recirculation from the exit shroud cavity were also plotted. When the exit shroud cavity has leakage to the impeller eye, the velocity peak at the impeller exit moves toward the center of the b2 width, where b2 is defined as the blade height at the impeller exit (see figure 2). However, the shroud leakage has only minor effects on the solution at r/rtip=1.0275 (Figure 4).

In Figure 4, the symbols represent experimental data, and the lines represent *Cm* distributions for the flow with vaneless space at the exit of the impeller.

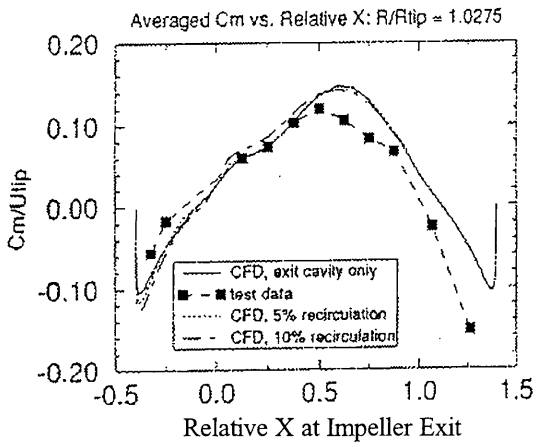

Figure 4. Comparison of circumferentially averaged meridional velocity at the impeller exit.

The test data shows that the peak is closer to the center of the b2 width. The discrepancy between the computed results and experimental data is partially due to the recirculation flow in the hub cavity. The leakage at the hub cavity leads to a stronger recirculation region, which shifts the velocity peak to the center of the b2 width. Since the CFD analysis did not include the leakage at the hub cavity, the predicted recirculation region in the vaneless space is not as strong as in the experimental study.

To simulate the entire turbopump including inducer, impeller, diffuser and volute, it is necessary to compute fully three-dimensional unsteady flow with components in relative motion. In the present study, the unsteady computing procedure for the entire turbopump has been developed using overset grid systems [9]. This capability is intended to provide a computational framework for analyzing rocket engine fuel and oxidizer supply system. Three-dimensional unsteady flow analysis with multiples of moving and stationary components require many physical time steps as well as a large number of grid points to resolve flow features of interest. Therefore, accelerating the computational procedure is of significant importance in engineering practice. One possibility of speed up comes from enhancements in computer hardware platforms, which at this time relies on parallel architecture. Advances in algorithms and efficient parallel implementations contribute to the other part of the speed-up. In the following, key elements in unsteady pump flow simulation are presented.

The pump used in liquid propulsion system may include various rotating and stationary components where the flow can be axial or centrifugal and extremely unsteady. A stand-alone inducer is often used to validate the flow solver used. In Figure 6, computed result of an inducer alone at a constant rotational speed is shown. A similar inducer was used later in VAD development.

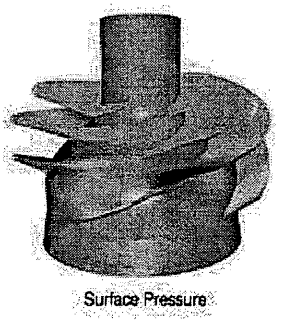

Figure 6. Surface pressure for a pump inducer.

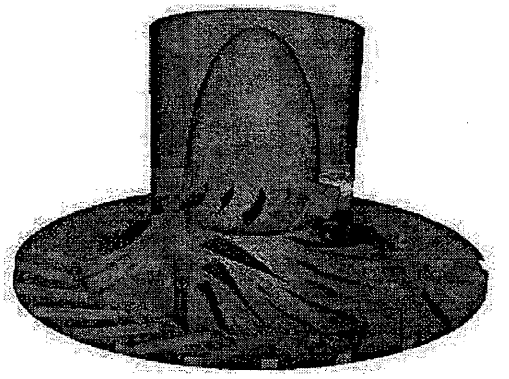

Figure 7. Geometry of a SSME pump including inlet guide vanes, impeller and diffuser blades.

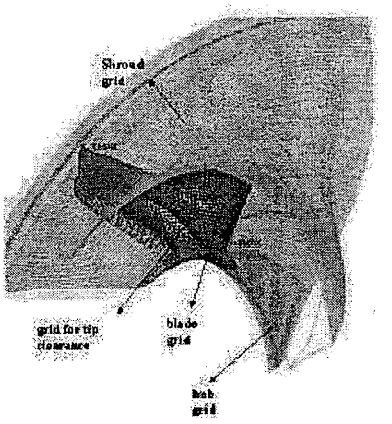

Figure 8. An overset grid system for the impeller blade section with tip clearance.

When rotating and stationary parts are included as shown in Figure 7, unsteady interactions between stationary and rotating components need to be included. To resolve the

complex geometry in relative motion, an overset grid approach is employed in the current effort. In this approach, a geometrically complex body is decomposed into a number of simple grid components. To illustrate this feature, the overset grid set up for the region around an impeller blade is shown in Figure 8. In order to solve the entire configuration including inlet guide vanes, impeller blades and diffuser blades, an overset grid system was constructed using 34.3 Million grid points with 114 zones in the present study. Since neighboring grids may overlap arbitrarily, these grids can be created independently from each other. Thus it is easier to generate high quality and nearly orthogonal grids using this approach. Connectivity between neighboring grids is established by interpolation at the grid outer boundaries. Addition of new components to the system and simulation of arbitrary relative motion between multiple bodies are achieved by establishing new connectivity without disturbing the existing grids.

Parallel computing strategies vary depending on computer architecture such as memory arrangement relative to processing units. Two approaches have been implemented in the present study: the first approach is hybrid MPI/OpenMP and the second one is Multi Level Parallelism (MLP) developed at NASA-Ames Research Center. The first approach is obtained by using massage-passing interface (MPI) for inter-zone parallelism, and by using OpenMP directives for intra-zone parallelism. INS3D-MPI is based on the explicit massage-passing interface across MPI groups and is designed for coarse grain parallelism. The primary strategy is to distribute the zones across a set of processors. During the iteration, all the processors would exchange boundary data between processors whose zones shared interfaces with zones on other processors. A simple master-worker architecture was selected because it is relatively simple to implement and it is a common architecture for parallel CFD applications. All I/O was performed by master MPI process and data was distributed to the workers. After the initialization phase is complete, the program begins its main iteration loop.

The second approach is obtained by using NAS-MLP routines. This approach differs from the MPI/OpenMP approach in a fundamental way in that it does not use messaging at all. All data communication at the coarsest and finest level is accomplished via direct memory referencing instructions. This approach also provides a simpler mechanism than MPI for converting legacy code, such as INS3D. For shared memory MLP, the coarsest level parallelism is supplied by spawning of independent processes via the standard UNIX fork. The advantage of the UNIX fork over MPI procedure is that the user does not have to change the initialization section of the large production code. Library of routines is used to initiate forks, to establish shared memory arenas, and to provide synchronization primitives. The boundary data for the overset grid system is archived in the shared memory arena by each process. Other processes access the data from the arena as needed. Figure 9 shows the scalability for SSME impeller computations using 19.2 Million grid points.

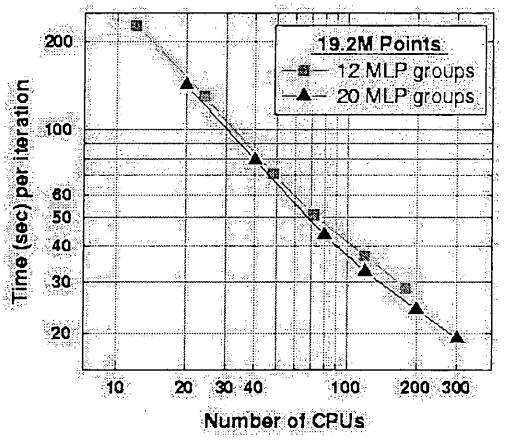

Figure 9. Time (sec) per iteration for SSME impeller computations.

Using both MPI/OpenMP hybrid approach and NAS-MLP parallel implementation, time-accurate computations of a pump shown in Figure 7 have been carried out on SGI Origin 2000 and 3000 platforms. Initially the flow was at rest and the impeller started to rotate impulsively. An instantaneous snapshot of particle traces and pressure surfaces from these computations are shown in Figure 10 after three full impeller rotations were completed. This procedure provides flow-field details not readily available from experiments. A full-length version of this work will be presented in a separate paper.

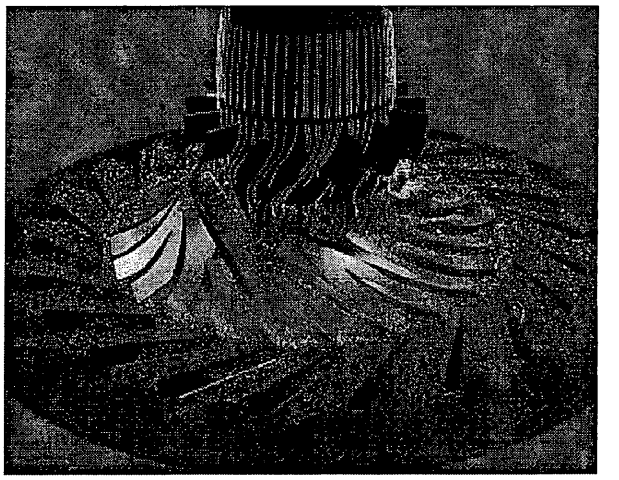

Figure 10. A snapshot of particle traces and pressure surfaces from unsteady turbopump computations.

BLOOD PUMP AS A VENTRICULAR ASIST DEVICE

In 1989, DeBakey Heart Center of the Baylor College of Medicine (BCM) began developing a new implantable VAD system jointly with NASA Johnson Space Center (JSC) [1]. This

LVAD is based on a fast rotating axial pump. In order to deliver the required blood flow rate, the rotational speed of this VAD is in the range of rocket pump operating condition. Therefore, the CFD procedures described earlier in conjunction with the rocket pump simulation was applied to this VAD development. By probing through computed results, regions of critical design interest can be identified such as regions of high turbulence shear flow which can damage the red blood cells and regions of re-circulation where blood clots may be formed. The ability to predict these phenomena expedited the development of the VAD.

First, the baseline VAD impeller was analyzed by solving the incompressible Navier-Stokes equations in a steady rotating frame of reference. Zonal multiblock grids were used in this component analysis.

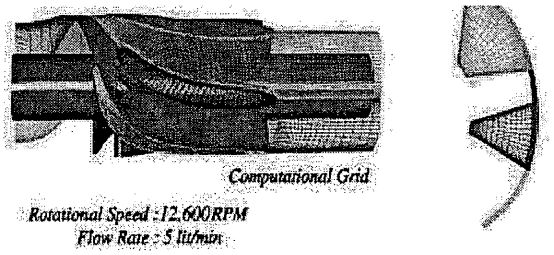

Figure 11. Computational grid for the baseline model of DeBakey VAD.

As shown in Figure 11, the computational domain is divided into five zones with grid dimensions of 127 x 39 x 33, 127 x 39 x 33, 59 x 21 x 7, 47 x 21 x 5, and 59 x 21 x 7, respectively. Zone 1 is the region between the suction side of the partial blade and the pressure side of the full blade; the region between the pressure side of the partial blade and the suction side of the full blade is filled by zone 2; and zones 3 through 5 allow tip-leakage effects to be included in the computational study and occupy the regions between the impeller blade tip and the casing. At the zonal interfaces, grid points were matched one-to-one. For all zones, an H-H type grid topology was used. An H-type surface grid was generated for each surface using an elliptic grid generator. The interior region of the three-dimensional grid was filled using an algebraic grid generator coupled with an elliptic smoother. Periodic boundary conditions were used at the end points in the rotational direction. The design flow of this impeller is 5 liters per minute and the design speed is 12,600 revolutions per minute (rpm). The problem was non-dimensionalized by the tube diameter (0.472 inches) and the impeller tip velocity. The solution was considered converged when the maximum residual had dropped at least five orders of magnitude.

A parametric study was performed to optimize the impeller blade shape and the tip clearance. The design shown in Figure 11 was analyzed with different tip clearances. However, the performance of the baseline design could not be brought up to the level required for human implantation both in blood cell damage level and the thrombus formation.

A modified designed was developed adding an inducer similar to the ones used in rocket pump. In collaboration with Micromed Technologies, NASA-JSC and BCM researchers, a new design consisting of the baseline impeller plus an inducer was investigated. Detail flow features and pump performances are compared for the two designs. The pressure gradient across the blades, and the pressure rise from inflow to outflow are compared in Figure 12. Blade geometry was then optimized in conjunction with detailed flow analysis.

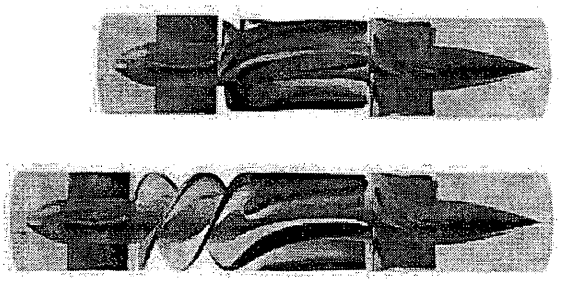

Figure 12. Pressure surfaces of the baseline design (top) and new impeller design (bottom).

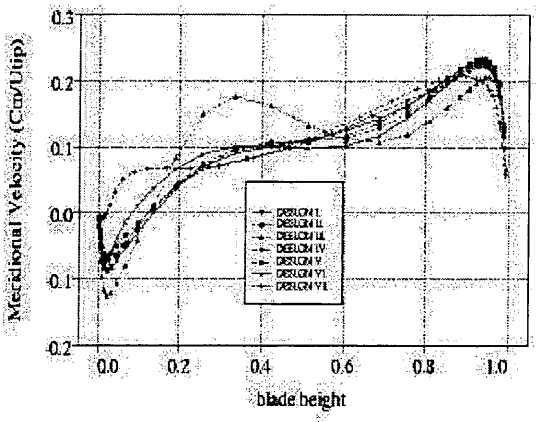

Figure 13. Meridional velocity distribution along impeller blade height of various designs.

In Figure 13, the circumferentially averaged meridional velocity distribution is shown along the blade height for various designs. The original blade design is referred to as Design I. Design II has less blade curvature than Design I in the trailing edge region, and Design III has more blade curvature than Design I. In Design IV, the blade shape for Design I is kept and the tip clearance is reduced. In Design V, the hub region has the blade shape for Design I and the tip region has the blade shape for Design II. In this design, the impeller blades have backward lean near the trailing edge region. In Design VI, the blades have forward lean which includes Design III in the hub region and Design I in the tip region. Design VII has small tip clearance gap, Design I blade shape and an inducer geometry upstream of impeller blades. In Figure 13, all designs except Design VII showed back flow near

the hub region. The back flow has been reduced with forward blade. In addition, the effects of tapered hub and diffuser angle are combined to minimize the back flow. Figure 14 shows the efficiency curves for these design variations. The inducer addition clearly shows substantial improvement in the hydrodynamic efficiency, at the same time provides a sufficient pressure rise to suppress cavitation.

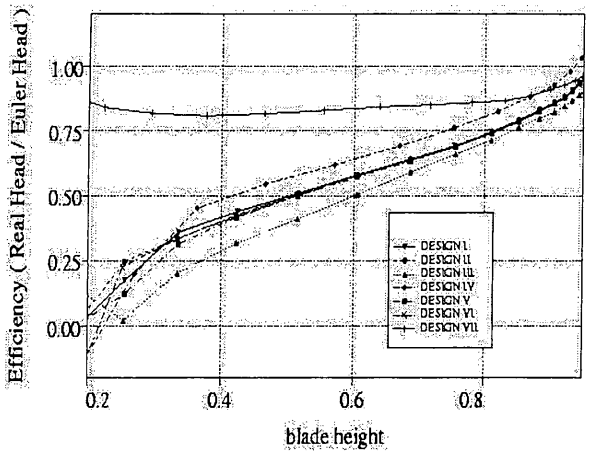

Figure 14. Hydrodynamic efficiency distribution along impeller blade height of various designs.

Besides improving the pumping efficiency, the design of the VAD requires good wall washing near the solid wall by reducing the stagnation regions. One of the critical regions for potential blood clotting is near the bearing area between rotating and non-rotating components. Clotting can be caused in the hub area due to either high shear or stagnation depending on the gap and configuration of the area.

Figure 15 shows velocity vectors colored by velocity magnitude for different bearing designs. Design 1 is the original baseline design with the cavity width of b. This design showed very high shear stresses near the rotating hub face and very stagnant fluid region in the lower portion of the cavity. Increasing the cavity width gradually up to 8b, circulation in the cavity is increased substantially. In order to eliminate stagnant areas in the lower portion of the cavity, the hub surface was then tapered which reduces the cavity height accelerating the flow near the hub region. This resulted in stronger wall washing in the cavity. A modified version of this configuration has been adopted in the current DeBakey VAD design.

In Figure 16, areas where the VAD design is improved by using CFD analysis is summarized.

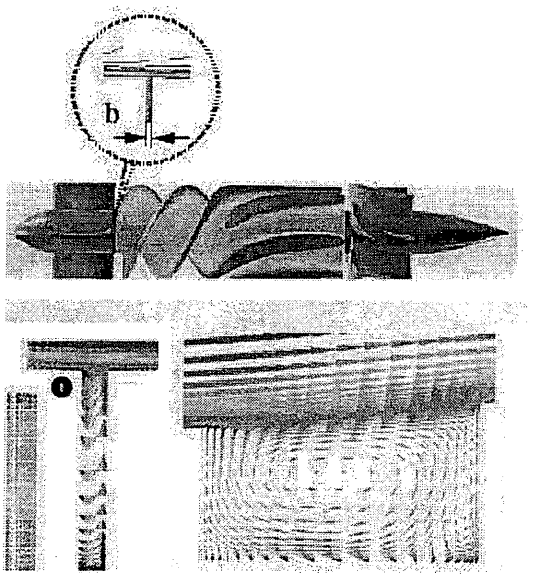

Figure 15. Velocity vectors inside the initial (left) and the final bearing geometry (right).

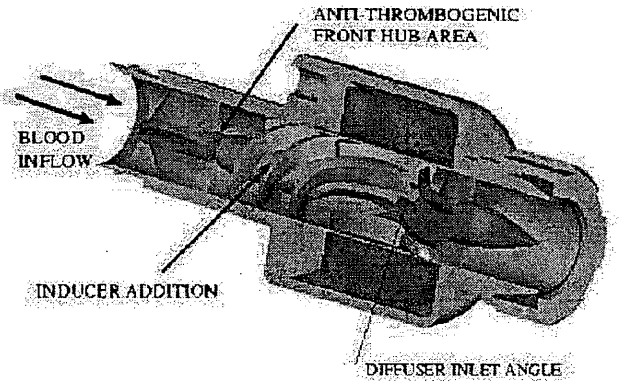

Figure 16. Contribution of CFD analysis to VAD design.

The performance of the new design is compared to the baseline design in Table 1 where the clinical results were obtained by BCM. The hemolysis index reported here shows the amount of hemoglobin generated by the pump in grams per 100 liters. Destruction of the red blood cells results in the release of hemoglobin. The new design shows a remarkable improvement in performance over the baseline design. There is a 22% increase in overall pumping efficiency. The performance of the new design was sufficiently improved resulting in a device implantable in human. The first human implantation was performed successfully in 1998 followed by applications to many other patients ever since.

	Baseline Design	New Design
Hemolysis Index	0.02	0.002
Thrombus Formation	Yes	no
Test Run Time	2 days	30+ days
Human Implantation		6+ months

Table 1. Clinical results for baseline and new designs of VAD.

SUMMARY

An efficient and robust solution procedure for 3-D turbopump analyses and its spin-off application to VAD impeller have been presented. The technique solves the viscous incompressible Navier-Stokes equations using the pseudo-compressibility method. A high-order accurate upwind differencing and an efficient implicit scheme are used in the flow solver. The flow simulation procedure was developed to analyze an advanced turbopump impeller and an SSME configuration. Validated solution procedure was then applied to the development of DeBakey VAD. Various design improvements were made through the use this computational tool. For example, an inducer addition dramatically increased pumping efficiency thereby reducing the hemolysis to an acceptable level for human use and an optimum cavity redesign practically removed thrombus formation in the bearing area. Overall the VAD development was expedited with the help of CFD technology originally developed for rocket pump, thus enabling human implantation. Overall performance has been demonstrated through successful human implantations.

ACKNOWLEDGEMENTS

The authors would like to thank Micromed Technologies, NASA JSC and Baylor College of Medicine VAD Team for providing the clinical results.

REFERENCES

1. Aber, G. S., Akkerman, J.W., Bozeman, R. J., and Saucier, D. R., "Development of The NASA / Baylor VAD," NASA Technology 2003 Conference, 1993.

2. Kiris, C., Rogers, S. E., Kwak, D. and Chang, I.D., "Computation of Incompressible Viscous Flows through Artificial Heart Devices with Moving Boundaries," *Fluid Dynamics in Biology*, Proceedings of an AMS-IMS-SIAM Joint Research Conference, ed. A. Y. Cheer and C. P. van Dam, American Mathematical Society, Providence, R. I., pp. 237-247 1991.

3. Quarteroni, A. "Modeling the Cardiovascular System-A Mathematical Venture: Part I," SIAM News, Volume 34, Number 5, 2001.

4. Kwak, D., Chang, J. L C., Shanks, S. P., and Chakravarthy, S., ``A Three-Dimensional Incompressible Navier-Stokes Flow Solver Using Primitive Variables," *AIAA Journal*, Vol. 24, No. 3, pp. 390-396, 1977.

5. Rogers, S. E., Kwak, D. and Kiris, C., "Steady and Unsteady Solutions of the Incompressible Navier-Stokes Equations," AIAA J. vol. 29, N0. 4, pp 603-610, April 1991.

6. Kiris, C., and Kwak, D., "Numerical Solution of Incompressible Navier-Stokes Equations Using a Fractional-Step Approach," Computers & Fluids, vol. 30, pp829-851, 2001.

7. Kiris, C., Chang, L., Kwak, D., and Rogers, S. E., "Incompressible Navier-Stokes Computations of Rotating Flows," AIAA Paper No. 93-0678, 1993.

8. Kiris, C. and Kwak, D., "Progress in Incompressible Navier-Stokes Computations for the Analysis of Propulsion Flows," NASA CP 3282, Vol. II, Advanced Earth-to-Orbit Propulsion Technology, 1994.

9. Kiris, C., Kwak, D., and Chan, W., "Parallel Unsteady Turbopump Simulations Using Overset Grid System," 5th Symposium on Overset Grids and Solution Technology, University of California at Davis, Davis, CA, September 18-20, 2000